Magnetic Resonance in Medicine 47:940–947 (2002)
DOI 10.1002/mrm.10147

MR Temperature Measurement in Liver Tissue at 0.23 T With a Steady-State Free Precession Sequence

D. Germain,[1,2] E. Vahala,[3] G.J. Ehnholm,[3] T. Vaara,[3] M. Ylihautala,[3] M. Savart,[1] A. Laurent,[1] J. Tanttu,[3] and H. Saint-Jalmes[4*]

MRI can be used for monitoring temperature during a thermocoagulation treatment of tumors. The aim of this study was to demonstrate the suitability of a 3D steady-state free precession sequence (3D Fast Imaging with Steady-State Precession, 3D TrueFISP) for MR temperature measurement at 0.23 T, and to compare it to the spin-echo (SE) and spoiled 3D gradient-echo (3D GRE) sequences. The optimal flip angle for the TrueFISP sequence was calculated for the best temperature sensitivity in the image signal from liver tissue, and verified from the images acquired during the thermocoagulation of excised pig liver. Factors influencing the accuracy of the measured temperatures are discussed. The TrueFISP results are compared to the calculated values of optimized SE and 3D GRE sequences. The accuracy of TrueFISP in the liver at 0.23 T, in imaging conditions used during thermocoagulation procedures, is estimated to be ±3.3°C for a voxel of 2.5 × 2.5 × 6 mm^3 and acquisition time of 18 s. For the SE and GRE sequences, with similar resolution and somewhat longer imaging time, the uncertainty in the temperature is estimated to be larger by a factor of 2 and 1.2, respectively. Magn Reson Med 47:940–947, 2002. © 2002 Wiley-Liss, Inc.

Key words: temperature; interventional MRI; SSFP sequence; liver tumors; thermoblation

The treatment of hepatic metastases by local heat delivery has drawn considerable interest over the last few years. The efficiency of thermoablation is improved if real-time monitoring of heat distribution is available during the treatment (1–3). At the moment, MRI is the only medical imaging modality that can provide noninvasive temperature information from tissue.

Temperature monitoring with MRI is possible using the temperature sensitivity of the proton resonance frequency, i.e., chemical shift (4), diffusion (5), or longitudinal relaxation time T_1 and equilibrium magnetization M_0 (6–8). The applicability of each method depends on the field strength of the MR scanner used, and on the target anatomy (9).

Low-field open magnets are well suited for performing tumor ablations. They offer maximum access to the patient; dedicated tools for interventional MRI, such as needle tracking systems and in-room controls; less-intense needle artifacts; and lower-cost procedures. A disadvantage is that temperature-measuring methods utilizing the temperature sensitivity of the proton resonance frequency are difficult to use, as the change in chemical shift is directly proportional to field strength. For example, the sensitivity is 6.5 times less sensitive at 0.23 T than at 1.5 T.

Motion artifacts hamper diffusion-based temperature measurement methods (10), making them impractical for use in the liver. With low-field open scanners, the easiest method for obtaining temperature data from the liver is to use the temperature dependence of T_1 and M_0. Their temperature sensitivity is still high at lower magnetic field strengths, and they are easily measurable with standard sequences and hardware.

The accuracy of temperature measurement with T_1 and M_0 depends strongly on the type of MR sequence used and on the choice of acquisition parameters, such as the repetition time (TR) and flip angle (α). Temperature resolution may be affected by a factor of 5, depending on the type of sequence used for the measurement (11). The parameters need to be carefully chosen to optimize the temperature measurement while maintaining a reasonable temporal and spatial resolution.

Spin-echo (SE) sequences, gradient-recalled acquisitions in the steady state (GRASS), and spoiled gradient-recalled acquisitions (SPGR) have been employed for monitoring temperature by using the temperature dependency of T_1 (7,8,11,12). A steady-state sequence (3D Fast Imaging with Steady-State Precession, 3D TrueFISP) offering a particularly high signal-to-noise ratio (SNR) per unit of time is an interesting alternative for temperature measurement. The sequence yields T_2/T_1-weighted images, which is beneficial for tumor ablation in liver for two reasons. First, it allows good visualization of the anatomy and certain types of pathologies, which is necessary for guiding the heating probe into place. Second, the T_1 dependency of the signal can be used for monitoring the temperature. Moreover, the TrueFISP sequence is inherently rather insensitive to motion (13), and very good results have been obtained when using it in low-field open magnets (14) during interventional procedures.

The aim of this study was to test a 3D TrueFISP sequence (13), optimized for temperature measurement, and to compare its suitability with optimized SE and gradient-echo (GRE) sequences. To do this, simulations and experimental validations were performed.

SIMULATION METHODS

The influence of temperature, via M_0 and T_1, on the MR image was simulated using mathematical models, which included noise. Parameters for three sequences—SE, GRE, and TrueFISP—were determined for optimal temperature monitoring.

[1]Center for Research in Interventional Imaging, Jouy en Josas, France.
[2]Marconi Medical Systems France, Chatenay Malabry, France.
[3]Marconi Medical Systems Finland, Vantaa, Finland.
[4]Laboratoire de RMN, Université Claude Bernard, Lyon, France.

Grant sponsor: Marconi Medical Systems France.

*Correspondence to: Hervé Saint-Jalmes, Laboratoire de RMN, Université Claude Bernard, 69622 Villeurbanne cedex, France.
E-mail: saint-jalmes@univ-lyon1.fr

Received 31 January 2001; revised 10 January 2002; accepted 10 January 2002.

Temperature Sensitivity of M_0

According to Curie's law, M_0 is proportional to the inverse of temperature ($-1/T$) (15). At normal body temperatures, M_0 decreases approximately linearly with temperature for all tissues. This corresponds to a coefficient of $k_{M_0} = -30\% \pm 0.01\%/°C$, $= -0.30 \pm 0.01\%/°C$, valid for the limited temperature range, to which the tissue is exposed during a thermocoagulation procedure.

Temperature Sensitivity of Relaxation Time Constants

The temperature sensitivity of T_1 varies depending on the tissue type and accumulated thermal destruction. It is a nonlinear function of temperature for all tissue types over the temperature range of 37–80°C (16,17). Above 65°C, the tissue destruction effects on the T_1 of the liver tissue become dominant and prevent accurate temperature measurement. Below 65°C, the sensitivity of T_1 has been measured, in vitro, for pig liver tissue at 0.23 T (12). As relaxation time constants are quite similar across species (18,19), this data can be used to assess temperature-induced changes in T_1 of a human liver:

$$T_{1h} = p_2 \cdot \Delta T^2 + p_1 \cdot \Delta T + T_{1b} = (p_{2N}\Delta T^2 + p_{1N}\Delta T + 1)T_{1b}$$
$$\text{with} \quad p_2 = 0.041\ ms°C^{-2} \quad \text{and} \quad p_1 = 2.071\ ms°C^{-1} \quad [1]$$

T_{1b} and T_{1h} are longitudinal relaxation time constants of the tissue before and during heating, respectively, and ΔT is the temperature difference from the baseline temperature of 37°C. Coefficients p_2 and p_1 are constants describing the temperature sensitivity of T_1 in liver tissue, which can be alternatively defined as p_{2N} and p_{1N} when normalized to the T_{1b} value. Note that the numerical values from Ref. 12 are here adjusted so that T_1 obeys the same second-order polynomial curve, but with the relative origin changed, i.e., $\Delta T = 0$ gives the T_1 value at our baseline temperature of 37°C, whereas in the original article a body temperature of 35°C was used.

The temperature sensitivity of T_2 in biological tissue has been considered negligible by most authors who have used T_1 for measuring temperature (7,8,11).

Theoretical Model for a 3D TrueFISP Signal Behavior as a Function of Temperature

A mathematical expression for the TrueFISP signal as a function of temperature is obtained by combining the equation for the signal with the temperature-dependent functions of T_1 and M_0. An equation for the signal can be found, valid with the following conditions: the TR should be much smaller than T_1 of the tissue, and the precession angle ϕ—defined as $\int \omega dt$, where integration is over TR and ω is the frequency offset from the Larmor frequency—should be equal to π, which is the condition for the maximum signal. Strictly speaking, the latter condition can only be met in an isothermal tissue, as the Larmor frequency is temperature-dependent. However, with the TR values used here, the temperature dependency of phase is not an issue for low-field magnets: the signal intensity change, due to an unaccounted phase error caused by a temperature difference that is less than 30°C, is below 1% in a 0.23 T magnet. So, the signal intensity S, measured with the 3D TrueFISP sequence, can be considered to follow the equation (13):

$$S(T) \approx \frac{M_0(T) \cdot \left(\dfrac{TR \cdot \sin\alpha}{T_1(T)} + \dfrac{\exp\left(-\dfrac{TR}{T_2}\right) \cdot TR \cdot \sin\alpha}{T_1(T)} \right)}{1 - \exp\left(-\dfrac{2TR}{T_2}\right) \cdot \left(1 - \dfrac{TR}{T_1(T)} - \cos\alpha\right) - \left(1 - \dfrac{TR}{T_1(T)}\right) \cdot \cos\alpha + \dfrac{\exp\left(-\dfrac{TR}{T_2}\right) \cdot TR \cdot (1 + \cos\alpha)}{T_1(T)}} \quad [2]$$

where T = temperature, α = flip angle, and TR = repetition time.

Temperature cannot be analytically solved from Eq. [2], so numerical methods must be used. The normalized signal S_N, i.e., signal intensity S_h at elevated temperature divided by the signal intensity S_b at the baseline temperature of 37°C, is plotted in Fig. 1 as a function of temperature (solid line). S_b and S_h were calculated using TR = 7.6 ms, TE = 3.8 ms, and flip angle = 63°. These are typical parameter values used for imaging liver in less than 30 s, which is a short enough acquisition time for apnea. T_{1b} was set to 240 ms and T_2 to 40 ms (commonly registered relaxation time constants in normal liver tissue at 37°C (18)). We see from the figure that the temperature dependence of S_N is quite linear. A straight line was fitted to the curve, according to the equation:

$$\Delta T = a + bS_N \quad \text{with} \quad a, b = f(\alpha, TR, k_{M_0}, p_1, p_2, T_{1b}), \quad [3]$$

where a and b are constants for a given tissue type, TR, and flip angle. The applicability of the linear approximation was examined by recalculating the theoretical curve for T_{1b} and T_2 values differing from those used in determining the linear approximation constants. The deviation between the linear approximation and theory was found to be small in comparison with the thermal noise, even with large changes in values (cf. Tables 3a and b, Fig. 4, and the Simulation Results section). Therefore, the dependence between normalized signal strength and temperature for the TrueFISP sequence is linear, with a precision that is better than the spread in values caused by noise, and thus we used this property in the calculations.

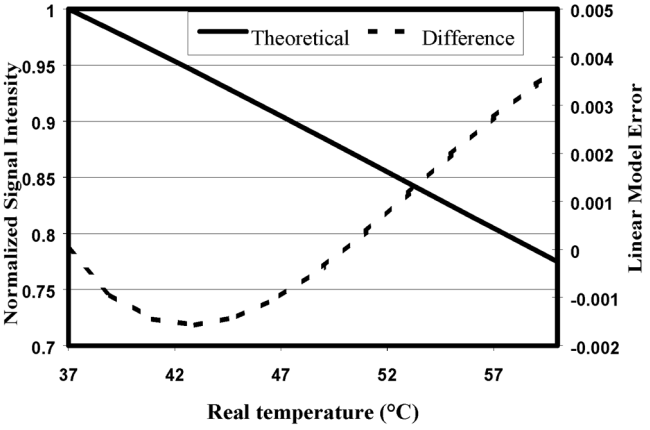

FIG. 1. The normalized signal behavior of 3D TrueFISP as a function of temperature (solid line), calculated using Eqs. [1] and [2]. The signal behaves nearly linearly, as shown by the error in the linear approximation (dotted line, the right axis scale). The reference temperature for the normalization was set to 37°C, with T_{1b} equal to 240 ms and T_2 to 40 ms. The sequence parameters are listed Table 1.

Optimization of the Flip Angle for Temperature Measurement With a 3D TrueFISP Sequence

The flip angle of the 3D TrueFISP sequence is a free parameter that can be varied in order to achieve the best temperature sensitivity (whereas the TR is already fixed) to achieve the desired acquisition time for the sequence.

The quantity one wants to maximize is the SNR in the temperature image, $\Delta T/\sigma_{\Delta T}$, where $\sigma_{\Delta T}$ is the standard deviation (SD) of a temperature change ΔT. The optimization should take into account two facts: First, the physical source of noise in the system comes from the dissipation in the coil and patient, and is independent of the flip angle, which only affects the signal. Second, the noise in the temperature, represented by the aforementioned $\sigma_{\Delta T}$, is produced via two images, namely the one taken as a reference at 37°C, and the one that corresponds to the increased temperature.

The temperature is determined from the normalized signal S_N. The SD, $\sigma_{\Delta T}$, is obtained from the corresponding quantity σ_{S_N} for S_N using the derivative of ΔT vs. S_N, which yields a simple result when the linear approximation of Eq. [3] is used:

$$\sigma_{\Delta T} = \left|\frac{\partial \Delta T}{\partial S_N}\right| \sigma_{S_N} \approx b\sigma_{S_N}. \quad [4a]$$

The SD σ_{S_N} is in turn obtained from the measured SD σ_S, which is the same for the reference signal S_b and the temperature-dependent signal S_h:

$$\sigma_{S_N} = S_b^{-2}\sqrt{S_h^2 + S_b^2}\cdot \sigma_S. \quad [4b]$$

The quantity to be optimized, $\Delta T/\sigma_{\Delta T}$, includes the factors M_{0b}, equilibrium magnetization at the baseline temperature of 37°C, and σ_S, which are independent of the optimized flip angle, cf. Eqs. [2]–[4]. We can then equally well use a derived figure of merit (FOM) that is independent of factors related to the scanner-dependent absolute signal and noise levels, i.e., an SNR function ($\Delta T/\sigma_{\Delta T}$) normalized with M_{0b}/σ_S. Accordingly, the optimization of the sequence consists of maximizing the following (20):

$$FOM = \frac{\Delta T S_b}{M_{0c}\sqrt{S_N^2 + 1}}\left|\frac{\partial \Delta T}{\partial S_N}\right|^{-1} \approx \frac{\Delta T S_b}{M_{0c} b\sqrt{S_N^2 + 1}}. \quad [5]$$

The FOM was calculated as a function of temperature and flip angle α with the same parameters that were used to generate Fig. 1. The maximum values with respect to α were determined, and a medium value within the temperature range was used as the optimal angle.

Theoretical Model for SE and 3D GRE Signal Behavior as a Function of Temperature

Mathematical expressions for the signal intensity measured with SE (S_{SE}) and 3D GRE (S_{GRE}) sequences are:

$$S_{SE}(T) = M_0(T)\exp(-TE/T_2)\{1 - \exp[-TR/T_1(T)]\}$$
$$\text{provided that } TR \gg T_2 \quad [6a]$$

$$S_{GRE}(T) = M_0(T)\exp(-\mathrm{TE}/T_2)\sin\alpha \times \frac{1 - \exp[-TR/T_1(T)]}{1 - \cos\alpha\exp[-TR/T_1(T)]}. \quad [6b]$$

Using simplification methods similar to those for the 3D TrueFISP, the equations for calculating the temperature become:

$$\Delta T(\mathrm{SE}) = a + bS_N \quad \text{with} \quad a, b = f(TR, k_{M_0}, p_1, p_2, T_{1b}) \quad [7a]$$

$$\Delta T(GRE) = a + bS_N \quad \text{with} \quad a, b = f(\alpha, TR, k_{M_0}, p_1, p_2, T_{1b}). \quad [7b]$$

Note that for an SE sequence, a and b depend on the TR, whereas for the 3D GRE they depend on the TR and flip angle α.

Optimization of SE and 3D GRE Sequences for Temperature Measurement

Maximizing the FOM of Eq. [5] with a variable flip angle optimizes a 3D GRE sequence for temperature measurement. S_b and S_h were calculated with a TR of 12 ms and TE of 4 ms from Eq. [6b]. The rest of the imaging parameters were common with 3D TrueFISP sequence.

For SE, the flip angle is omitted from Eq. [7a] because standard SE sequences use a constant flip angle of 90° for maximum signal. Only the TR is used as an optimization parameter. Because acquisition time is proportional to TR, the parameter has to be optimized to allow the most efficient temperature measurement in a limited amount of time. A new optimization function, $\mathrm{OF}_{\Delta T}(\mathrm{SE})$, is defined to optimize SNR in temperature images per unit of time. As the SNR is proportional to the square root of the accumulated time, $OF_{\Delta T}(\mathrm{SE}) = FOM/\sqrt{TR}$ (20), where FOM is the figure of merit defined in Eq. [5]. In the calculations, S_b and S_h were evaluated from Eq. [6a] with a TE of 20 ms, T_1

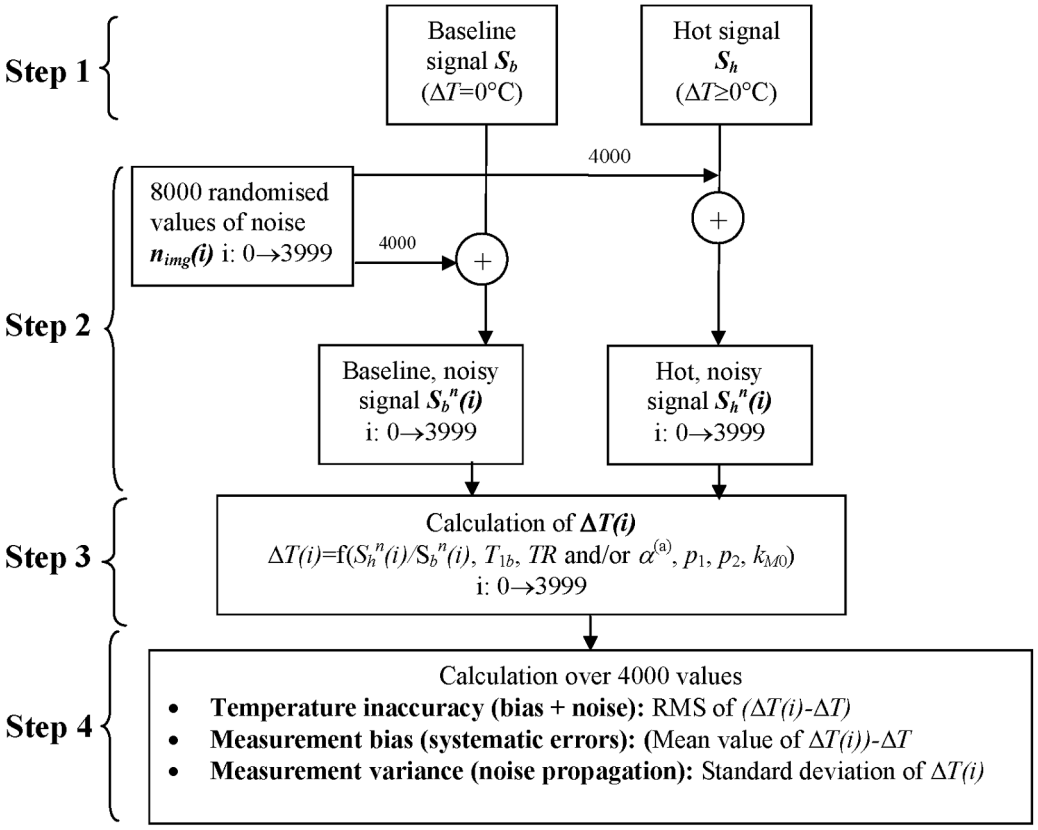

FIG. 2. Simulation of the behavior of MR signal and noise for estimating the accuracy of temperature measurement with SE, 3D GRE, and 3D TrueFISP sequences. Random noise was added to signal values calculated for hot and baseline samples. Temperature was then calculated with the noisy values. Simulated temperature increase steps were +0, +5, +10, +15, +20, +25, +30, and +35°C. The impact of systematic bias and noise on the measurement accuracy were evaluated both together and separately. aΔT depends on TR and/or α depending on the sequence used; cf. Eqs. [3], [7a], and [7b].

and T_2 set to 240 ms and 40 ms, respectively, and TR constrained to the range of 40–1000 ms.

Computer Simulation of Optimized SE, 3D GRE, and 3D TrueFISP Sequences

Simulation of the MR signal behavior as a function of temperature was performed for each type of sequence with models built with Mathematica 3.0 (Wolfram Research, Champaign, IL). The diagram of the simulation is shown in Fig. 2.

Step 0: Preliminary Measurements

SE, 3D GRE, and 3D TrueFISP images of the liver of a healthy volunteer were acquired in order to get realistic signal (S_b), noise (n_{img}), and equilibrium magnetization (M_{0b}) values from the liver at a body temperature of approximately 37°C. Data acquisition was done on an open 0.23 T scanner (Proview, Marconi Medical Systems). The receiver coil was a multipurpose loop coil with a diameter of 42 cm. Acquisitions were performed during apnea. Sequence parameters are described in Tables 1 and 2. The measured values and sequence parameters were used in subsequent simulation steps.

Step 1: Generation of MR Signals

The MR signal of heated liver, S_h, was calculated using Eqs. [2], [6a], and [6b] for 3D TrueFISP, SE, and 3D GRE, respectively, together with temperature-dependent M_0 and T_1. Relaxation time constants were estimated with a T_{1b} of 240 ms and T_2 of 40 ms (commonly registered relaxation time constants in normal liver tissue at 37°C (18)).

Table 1
MR Parameters of SE, 3D GRE, and 3D TrueFISP Images

	SE	3D GRE	3D TrueFISP
TR (ms)	TR_{opt}[a]	12	7.6
TE (ms)	20	4	3.8
Flip angle (°)	90	α_{opt}[a]	α_{opt}[a]
FOV (mm)		320	
Matrix (pixels)		128 × 128	
Slice thickness (mm)		6	
Number of slices	6	8	8
Acquisition time (s)	27	31	18

The images from a volunteer gave an estimate for typical SNR in a minimally invasive thermoablation.
[a]Parameters optimized for temperature measurement in liver.

Table 2
Simulation Data

	SE	3D GRE	3D TrueFISP
Optimized parameters	TR_{opt} = 214 ms	α_{opt} = 26°	α_{opt} = 63°
ΔT approximation	106.8 ± 0.3 (1 − S_N)	102.4 ± 0.2 (1 − S_N)	103.8 ± 0.2 (1 − S_N)

Optimized MR acquisition parameters and equations for calculating temperature increase (Eqs. [3], [7a], and [7b]) in liver for 3D TrueFISP, SE, and 3D GRE, using acquisition parameters shown in the Table 1.

Step 2: Generation of Noise

Random values of white Gaussian noise, n_{img}, were added to S_h and S_b, resulting in noisy sets of data, S_h^n and S_b^n. Noise was scaled so that the SNR in the sets at 37°C was identical to the SNR in corresponding volunteer images of step 0.

Step 3: Temperature Calculation

The ΔT values were calculated with Eqs. [3], [7a], and [7b] for 3D TrueFISP, SE, and 3D GRE sequences, respectively. The coefficients of the equations were determined by fitting the linear models to their corresponding theoretical curves calculated from Eqs. [2], [6a], and [6b].

Step 4: Statistics

Inaccuracy in temperature measurement was assessed with the root mean square (RMS) of the difference between the temperature used in calculating the set and simulated noisy temperature. It contains both noise and systematic bias. The systematic bias due to mathematical simplifications, i.e., the linear approximations, was assessed separately by calculating the difference between the temperature used in calculating the set and mean simulated noisy temperature. The random noise in the measurements was calculated with the SD.

Steps 1–4 were repeated for ΔT = 0, 5, 10, 15, 20, 25, 30, and 35°C. This corresponds to tissue temperature varying from 37°C to 72°C. Above approximately 65°C, experimentally determined temperatures would of course become uncertain because of the tissue destruction effect mentioned above.

Experimental Methods

Two in vitro studies with the 3D TrueFISP sequence were carried out on a 0.23 T open magnet (Proview, Marconi Medical Systems). One aimed at validating the results of temperature accuracy simulations, the other aimed at validating the optimization method used for the flip angle. A multipurpose loop coil (∅14 cm) was used for imaging samples of fresh extracted pig liver placed in test tubes. A priori, a 3D TrueFISP reference image was acquired with the sample stabilized at 37°C. The temperature of a sample was monitored with thermocouples while it was heated to a temperature between 35°C and 60°C. The temperature was stabilized and the TrueFISP acquisition repeated. Higher temperatures, e.g., up to 65°C, were not used because the measuring equipment could not then provide a stable and homogeneous temperature distribution over the whole sample. The parameters for the 3D TrueFISP acquisitions were the same as those described in Table 1.

In the first study, temperature increase was averaged over four pixels located at the tip of the thermocouple. The accuracy of measurements was assessed by calculating the RMS for the difference between temperature increase measured with the thermocouple and MR.

In the second study, a flip angle that maximized temperature accuracy was examined. The liver sample was heated to 45°C and 55°C. At both temperatures, 3D TrueFISP images were acquired with a flip angle that was varied from 30° to 90°. Temperature was calculated for each flip angle value using Eq. [3]. A measure for accuracy was obtained from the resulting temperature images by measuring the SD in a region of interest (ROI) of 15 pixels, located at the tip of the thermocouple.

SIMULATION RESULTS

The optimization FOM for 3D TrueFISP is shown as a function of temperature and flip angle in Fig. 3. At about 50°C, we find an optimal flip angle of 63°. This was selected as a median value within the temperature range that is generated during a thermocoagulation procedure. It is valid with good accuracy over the whole range, as can be seen from the flatness of the optimization surface.

Acquisition parameters optimizing the SE and 3D GRE sequences for temperature measurements in the liver were defined in a similar manner, and equations for calculating

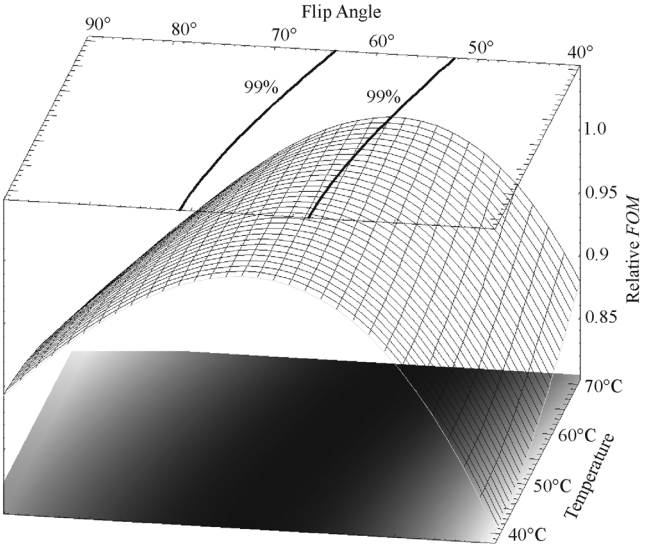

FIG. 3. FOM for flip angle optimization of 3D TrueFISP. The FOM is normalized with its maximum value at each temperature for presentational clarity. Two contour lines (thick solid lines) indicate an area where the FOM is within 99% of its maximum.

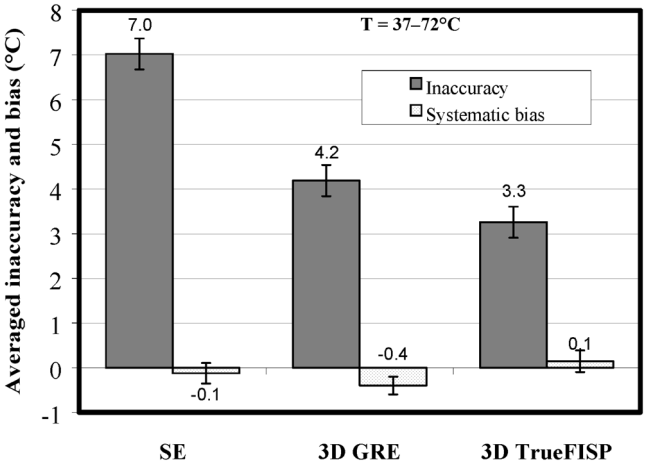

FIG. 4. Simulation data. Inaccuracy and bias of the calculated temperature at the temperature range of 37–72°C, when using simulated signals from SE, 3D GRE, and 3D TrueFISP. Inaccuracy is determined as the SD of the simulated points from the real temperature, and the bias is the difference between the mean and real temperatures. Note that the inaccuracy includes both noise propagation and bias due to systematic errors.

temperature increase were expanded in numerical form (cf. Table 2).

Inaccuracy and systematic bias in temperature, simulated with optimized SE, 3D GRE, and 3D TrueFISP in the temperature range of 37–72°C, are represented in Fig. 4. Inaccuracy was determined as the SD of the simulated points from the real temperature, and the bias as the averaged difference between the mean and real temperatures.

Temperature inaccuracy with TrueFISP was 3.3°C (acquisition time 18 s). This is 50% of the inaccuracy obtained with SE images (27 s), and 80% of the value for spoiled 3D GRE images (31 s). Error bars in Fig. 4 represent the SDs of the temperature inaccuracy and the bias in the temperature range 37–72°C. Systematic bias, introduced by the linear approximations in the model, represents less than 2% of the total error in temperature simulated for the SE sequence, 10% for GRE, and 3% for TrueFISP, which can be considered negligible in all three cases. As the linear models were fitted with T_{1b} = 240 ms and T_2 = 40 ms, additional systematic bias will be introduced if the T_{1b} and T_2 values of tissue differ from the predefined values. This effect was examined by varying T_{1b} and T_2 values and calculating ΔT with coefficients fitted with the original T_{1b} and T_2 values. The resulting systematic bias values are described in Table 3a and b. It should be noted that changing the relaxation time constants as much as 30% still results in errors that are of the same order of magnitude as the SD of temperature change in the sequences (3–7°C, see Fig. 4).

EXPERIMENTAL RESULTS

The MR-determined temperatures were calculated using the linear approximations with the values found in the simulations (Table 2). The normalized signal intensity was obtained by comparing signal intensity of a heated sample to that of the sample at 37°C. Figure 5 shows the temperature of extracted liver samples determined with 3D TrueFISP, using the optimal flip angle of 63°, vs. the value measured with a thermocouple. The RMS error within the measured temperature range was 1.6°C. Compared to the simulation results (~3°C), and taking into account the different noise levels (in simulations the noise level was four times larger), the noise has doubled from the expected value. Figure 6 shows the effect the flip angle has on the noise in temperature measurement. The minimum of the second-order polynomial curve fitted to the measured points is at 63° ± 8°, which agrees well with the optimized flip angle of 63° found in the simulations.

Table 3a
Simulation Data

T_1 (ms)	SE bias (°C)	3D GRE bias (°C)	3D TrueFISP bias (°C)
144	−2,5	−2,0	−1,5
168	−1,7	−1,5	−1,0
192	−1,1	−1,1	−0,6
216	−0,5	−0,7	−0,2
240	−0,1	−0,4	0,1
264	0,3	−0,2	0,3
288	0,6	0,1	0,6
312	0,9	0,3	0,8
336	1,1	0,5	0,9

Systematic bias in calculated temperatures between 37° and 72°C, induced by changing T_{1b} from the initial value of 240 ms. Bias represents the maximum temperature error of the optimized linear model (see Table 2) that is found within the temperature range.

DISCUSSION AND CONCLUSIONS

Simulations indicate that the 3D TrueFISP sequence is able to measure the temperature with twice the accuracy of SE, and 20% more accurately than with 3D GRE, whereas the acquisition time of 3D TrueFISP images is 33% and 42% shorter, respectively. The use of 3D imaging allows visualization of heat distribution in the volume of interest, and does not suffer from errors associated with the variation of flip angle over the slice profile.

Table 3b
Simulation Data

T_2 (ms)	3D TrueFISP bias (°C)
24	2,8
28	2,1
32	1,5
36	1,0
40	0,5
44	−0,6
48	−1,1
52	−1,7
56	−2,2

Systematic bias in calculated temperatures between 37° and 72°C, induced by changing T_2 from the initial value of 40 ms. Bias represents the maximum temperature error of the optimized linear model (see Table 2) that is found within the temperature range. Note that SE and 3D GRE have simple, exponential T_2-dependencies. Hence the relative signals, such as the calculated temperature, are unaffected by T_2 changes.

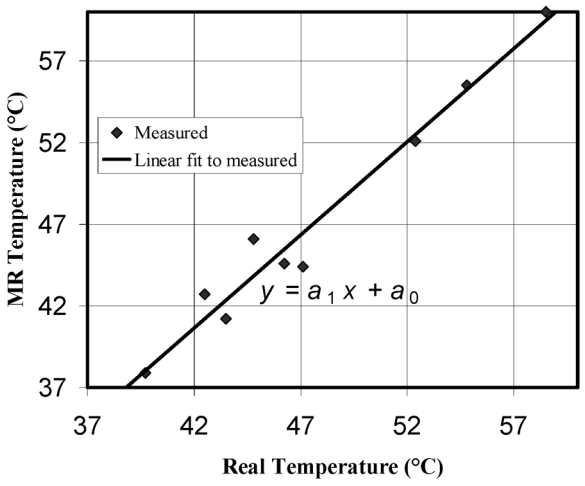

FIG. 5. Temperature data, measured with 3D TrueFISP from extracted liver samples. Each data point is an average of four pixels located at the tip of the thermocouple that tracks the real temperature. The solid line represents a linear fit to the measured data: a_1 = 1.14°C ± 0.08°C, and a_0 = –7.25°C ± 3.9°C.

Using the RMS error for the difference between the calculated temperature and actual temperature, as measured by the thermocouples or known a priori in the simulations, allowed the acquisition of error estimates that take into account not only measurement noise, but also the systematic error sources, such as those produced by the mathematical simplifications. Systematic errors due to simplifications were quite negligible and justified the use of the linearized equations. For example, the linear model for 3D TrueFISP resulted in a systematic bias that was less than 1°C in the typical temperature range for ablations.

The simple optimization procedure presented here can be used for optimizing T_1-weighted MR sequences for temperature measurements. It can also be extended for optimizing MR sequences for other measurements, and allows easy comparison of different types of sequences with different MR acquisition parameters. The optimization of the flip angle of a 3D TrueFISP sequence was straightforward and yielded a valid result, as confirmed by the experiments in which heated ex vivo liver samples were used.

During a thermal ablation, tissue is exposed to very steep temperature gradients of about 4°C/mm (12). Therefore, with a temperature accuracy of 3.3°C, as derived from Fig. 4 for in vivo conditions with 3D TrueFISP images, it is possible to localize a temperature front with a spatial resolution of approximately 2 mm. When treating liver metastases, a security margin of 5–10 mm of normal tissue must be destroyed in order to avoid recurrence (21). For this purpose, an inaccuracy of 2 mm in the localization of the isotherms seems acceptable.

Young et al. (22) reported that the changes in the in vivo perfusion, induced by the temperature increase, affect temperature measurements with T_1 and M_0 during hyperthermia. The reduction of the exposure time of a thermocoagulation procedure should minimize the effect of physiological changes that would then have less time to develop. It has been demonstrated that the size of the thermocoagulation lesions could be significantly increased by reducing the liver blood flow pharmacologically, or by the balloon occlusion of the portal vein and/or celiac and hepatic arteries (23–25). If thermocoagulation procedures are performed when liver perfusion is reduced, the effects of perfusion changes during the heating are reduced as well. However, further experiments must be performed in vivo to validate the method of temperature measurement with TrueFISP.

Errors in T_{1b} measurement do not greatly affect the accuracy of temperature measurements. For example, with a 30% error, the TrueFISP sequence experiences a bias of ~1°C, so there is little need for further improvements on the T_1 measurement.

Equations [4a] and [4b] indicate that noise in temperature images is proportional to noise in MR images. This means that doubling the SNR of the MR images causes a proportional improvement in temperature-measurement accuracy. In the simulation study, the SNR of simulated signals was the same as the SNR measured in vivo in the liver of a volunteer, using a large, multipurpose loop coil. Using a more suitable coil would improve the SNR of MR images significantly and result in improved temperature accuracy.

The temperature inaccuracy calculated in the simulation was a little over two times higher than the actual measurement value of 1.6°C using extracted liver samples. However, the SNR was four times lower. This discrepancy is most probably due to the heterogeneity of the extracted samples and the edge artifacts from the test tubes. It should also be noted that the field inhomogeneity affects the contrast of a TrueFISP sequence and the applicability of Eq. [2] if the phase condition is violated. Therefore, the working volume should be limited and the magnet shimmed carefully. This discrepancy serves to illustrate the importance of taking into account the changes encountered when moving from ex vivo to in vivo imaging. The 3D TrueFISP sequence allowed temperature measurement with an inaccuracy of 1.6°C in extracted liver tissue. However, if we consider in vivo imaging of a volunteer, with a large coil and physiological activity, the SNR of the MR images is smaller than that in ex vivo experiments.

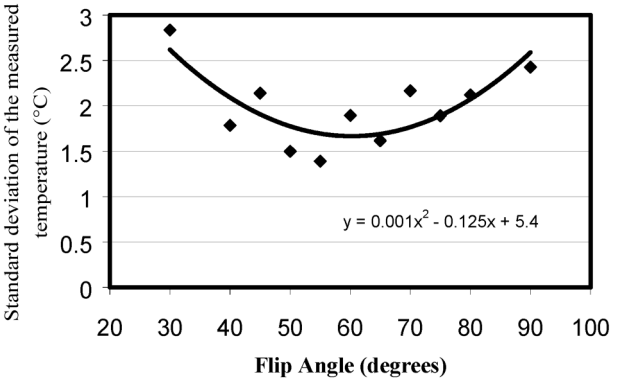

FIG. 6. SD in 3D TrueFISP temperature measurements vs. the flip angle from the ex vivo experiments. The data is a combination of two measurement series at 45°C and 55°C. The polynomial curve fitted on the measured data points has a minimum at the flip angle of 63° ± 8° (the "optimal angle"), and a correlation coefficient $R^2 \approx$ 0.7. Each data point of the experimental curve corresponds to the SD from an ROI of 15 pixels.

ACKNOWLEDGMENTS

D.G. is the recipient of a Marconi Medical Systems France grant.

REFERENCES

1. Vogl TJ, Mack MG, Muller PK, Straub R, Engelmann K, Eichler K. Interventional MR: interstitial therapy. Eur Radiol 1999;9:1479–1487.
2. Vogl TJ, Muller PK, Mack MG, Straub R, Engelmann K, Neuhaus P. Liver metastases: interventional therapeutic techniques and results, state of the art. Eur Radiol 1999;9:675–684.
3. Hall-Craggs MA. Interventional MRI of the breast: minimally invasive therapy. Eur Radiol 2000;10:59–62.
4. De Poorter J. Noninvasive MRI thermometry with the proton resonance frequency method: study of susceptibility effects. Magn Reson Med 1995;34:359–367.
5. Le Bihan D, Delannoy J, Levin RL. Temperature mapping with MR imaging of molecular diffusion: application to hyperthermia. Radiology 1989;171:853–857.
6. Parker DL, Smith V, Sheldon P, Crooks LE, Fussell L. Temperature distribution measurements in two-dimensional NMR imaging. Med Phys 1983;10:321–325.
7. Cline HE, Hynynen K, Hardy CJ, Watkins RD, Schenck JF, Jolesz FA. MR temperature mapping of focused ultrasound surgery. Magn Reson Med 1994;31:628–636.
8. Bohris C, Schreiber WG, Jenne J, Simiantonakis I, Rastert R, Zabel HJ, Huber P, Bader R, Brix G. Quantitative MR temperature monitoring of high-intensity focused ultrasound therapy. Magn Reson Imaging 1999; 17:603–610.
9. Quesson B, de Zwart JA, Moonen CT. Magnetic resonance temperature imaging for guidance of thermotherapy. J Magn Reson Imaging 2000; 12:525–533.
10. MacFall J, Prescott DM, Fullar E, Samulski TV. Temperature dependence of canine brain tissue diffusion coefficient measured in vivo with magnetic resonance echo-planar imaging. Int J Hyperthermia 1995;11: 73–86.
11. Matsumoto R, Mulkern RV, Hushek SG, Jolesz FA. Tissue temperature monitoring for thermal interventional therapy: comparison of T1-weighted MR sequences. J Magn Reson Imaging 1994;4:65–70.
12. Germain D, Chevallier P, Laurent A, Savart M, Wassef M, Saint-Jalmes H. MR monitoring of laser-induced lesions of the liver in a low field open magnet: temperature mapping and lesion size prediction. J Magn Reson Imaging 2001;13:42–49.
13. Zur Y, Wood ML, Neuringer LJ. Motion-insensitive, steady-state free precession imaging. Magn Reson Med 1990;16:444–459.
14. Duerk JL, Lewin JS, Wendt M, Petersilge C. Remember true FISP? A high SNR, near 1-second imaging method for T2-like contrast in interventional MRI at .2 T. J Magn Reson Imaging 1998;8:203–208.
15. Abragam A. The principles of nuclear magnetism. Oxford: Oxford University Press; 1961.
16. Lewa CJ, Majewska Z. Temperature relationships of proton spin-lattice relaxation time T1 in biological tissues. Bull Cancer 1980;67:525–530.
17. Graham SJ, Bronskill MJ, Henkelman RM. Time and temperature dependence of MR parameters during thermal coagulation of ex vivo rabbit muscle. Magn Reson Med 1998;39:198–203.
18. Bottomley PA, Foster TH, Argersinger RE, Pfeifer LM. A review of normal tissue hydrogen NMR relaxation times and relaxation mechanisms from 1–100 MHz: dependence on tissue type, NMR frequency, temperature, species, excision, and age. Med Phys 1984;11:425–448.
19. Lewa CJ, de Certaines JD. Measurements of the effect of storage at various temperatures on the T1 of ex vivo tissues. Med Phys 1995;22: 831–834.
20. Le Roux A. Cartographie de température en IRM: étude des phénomènes physiques, application à l'imagerie in vivo. Paris, France: Paris 11, Kremlin Bicêtre; 1994.
21. Solbiati L. New applications of ultrasonography: interventional ultrasound. Eur J Radiol 1998;27(Suppl 2):S200–S206.
22. Young IR, Hand JW, Oatridge A, Prior MV. Modeling and observation of temperature changes in vivo using MRI. Magn Reson Med 1994;32: 358–369.
23. Goldberg SN, Hahn PF, Halpern EF, Fogle RM, Gazelle GS. Radiofrequency tissue ablation: effect of pharmacologic modulation of blood flow on coagulation diameter. Radiology 1998;209:761–767.
24. Goldberg SN, Hahn PF, Tanabe KK, Mueller PR, Schima W, Athanasoulis CA, Compton CC, Solbiati L, Gazelle GS. Percutaneous radiofrequency tissue ablation: does perfusion-mediated tissue cooling limit coagulation necrosis? J Vasc Interv Radiol 1998;9:101–111.
25. Chen L, ter Haar G, Hill CR, Dworkin M, Carnochan P, Young H, Bensted JP. Effect of blood perfusion on the ablation of liver parenchyma with high-intensity focused ultrasound. Phys Med Biol 1993; 38:1661–1673.